

Banner appropriate to article type will appear here in typeset article

Scalar mixing in non-Markovian homogeneous isotropic synthetic turbulence

Pratyush S. Awasthi, Joaquim P. Jossy, Amitabh Bhattacharya and Prateek Gupta,[†]

Department of Applied Mechanics, Indian Institute of Technology Delhi, Hauz Khas, New Delhi, 110017, India.

(Received xx; revised xx; accepted xx)

We show that non-Markovianity of the velocity field is an essential property of turbulent mixing. We demonstrate this via passive scalar mixing by synthetically generated stochastic velocity fields. Including a separate velocity decorrelation time scale for each spatial scale (random sweeping) yields an essentially non-Markovian velocity field with a finite time memory decaying as τ^{-5} (for a decaying spectrum) instead of an exponential decay (Markovian), which is obtained by including a constant time scale for all spatial scales, irrespective of the filtering function. We characterize the Lagrangian mixing statistics of both the Markovian and non-Markovian synthetic fields and compare them against a corresponding incompressible direct numerical simulation (DNS). We also study diffusive passive scalar mixing in the Schmidt number range $Sc \leq 1$ using the DNS and the synthetic fields. While both the synthetic fields recover the $-17/3$ scalar spectrum for low Schmidt numbers, the mean gradients in a decaying simulation, as well as the production and dissipation of scalar variance in a statistically stationary simulation, are severely underpredicted by the Markovian fields compared to the non-Markovian fields. Throughout, we compare our results with companion 3D DNS to show the necessity of non-Markovianity in synthetic fields to capture mixing dynamics.

Key words:

1. Introduction

Mixing refers to the dynamic process by which the scalar gradients are redistributed and homogenized through the combined action of stirring and molecular diffusion (Zhou 2024; Jossy & Gupta 2025). Action of stirring by turbulence can be studied in statistically stationary systems with imposed concentration gradients (Yeung & Sreenivasan 2014), as well as decaying systems, in which the homogenization of an initially inhomogeneous field of concentration is studied (Yeung & Sreenivasan 2013). In steady mixing setups, the balance between stirring and diffusion signifies mixing. In contrast, unsteady mixing setups are characterised by stirring dominated mixing followed by diffusion dominated smoothening.

[†] Email address for correspondence: prgupta@iitd.ac.in

In this study, we elucidate the effect of temporal correlations on the mixing dynamics of both steady and unsteady mixing setups.

Advection of small-scale eddies in a turbulent flow by large, energy-containing eddies is called the random sweeping effect (Tennekes 1975). Using DNS, Gorbunova *et al.* (2021) showed that the decorrelation time decays as k^{-1} at large wavenumbers, rather than the classical $k^{-2/3}$, indicating that the large-scale eddies determine the temporal decorrelation. For homogeneous isotropic turbulence (HIT), Tennekes (1975) demonstrated that the Eulerian time spectrum exceeds its Lagrangian counterpart at high frequencies. Building on this idea, Yeung & Sawford (2002) used the random-sweeping framework to elucidate Lagrangian statistics relevant to mixing and dispersion, and showed that the concept extends to passive scalars. A Lagrangian measure of enhanced stirring is the exponential stretching captured by local finite-time Lyapunov exponents (FTLEs) (Aref 2020; Toussaint *et al.* 2000). Götzfried *et al.* (2019) compared passive-scalar mixing in both Eulerian and Lagrangian descriptions and showed that the mean mixing time – defined as the duration over which stirring dominates in unsteady mixing setups – is governed by the compressive local FTLE.

Synthetic turbulent fields aim to reproduce the essential dynamical features of turbulence while avoiding the computational cost associated with solving the full Navier–Stokes equations. Beyond practical utility, such models provide valuable insights into the intrinsic mechanisms of turbulence (Juneja *et al.* 1994). Batchelor *et al.* (1959) predicted that, at high Reynolds numbers and low scalar diffusivity, HIT produces a passive-scalar spectrum with the characteristic $-17/3$ scaling in the diffusive (viscous–convective) range. Holzer & Siggia (1994) demonstrated that two-dimensional, stochastically generated Gaussian velocity fields are able to reproduce this $-17/3$ scaling when used to mix passive scalars. Jossy *et al.* (2025) extended this synthetic-field framework to three dimensions, but found that such fields do not replicate the stirring efficacy of Navier–Stokes-generated turbulent flows. In this work, we formulate the synthetic generation of homogeneous isotropic turbulent fields capable of replicating the mixing efficiency of non-synthetic turbulent fields. In this work, we show that non-Markovian three-dimensional homogeneous synthetic velocity fields are closer to turbulence in mixing passive scalars than earlier developed Markovian fields. In the next section, we outline the theoretical basis for constructing non-Markovian synthetic fields and describe the numerical implementation. We then discuss the results in § 3 followed by a summary of findings in § 4.

2. Theory and numerical simulations

2.1. 3D time correlated non-Markovian synthetic field

Careta *et al.* (1994) proposed a two dimensional homogeneous isotropic velocity field using the Ornstein–Uhlenbeck process. Jossy *et al.* (2025) extended the methodology to generate three dimensional homogeneous isotropic velocity field. In this work, we extend the 3D synthetic velocity field proposed by Jossy *et al.* (2025) to generate a 3D non-Markovian homogeneous isotropic velocity field. We define a vector potential $\hat{\eta}(\mathbf{k}, t)$ in the spectral space which is an Uhlenbeck–Ornstein process with different decaying time scales given as,

$$\frac{d\hat{\eta}(\mathbf{k}, t)}{dt} = -\frac{\hat{\eta}(\mathbf{k}, t)}{\tau(\mathbf{k})} + \frac{\hat{Q}(\mathbf{k})}{\tau(\mathbf{k})} \hat{\chi}(\mathbf{k}, t), \quad (2.1)$$

where $\tau(\mathbf{k})$ is the spectrally varying time scale, $\hat{Q}(\mathbf{k})$ is the filtering kernel used to achieve a desired energy spectrum, and $\hat{\chi}(\mathbf{k}, t)$ is the Fourier transform of $\chi(\mathbf{r}, t)$ which is a delta

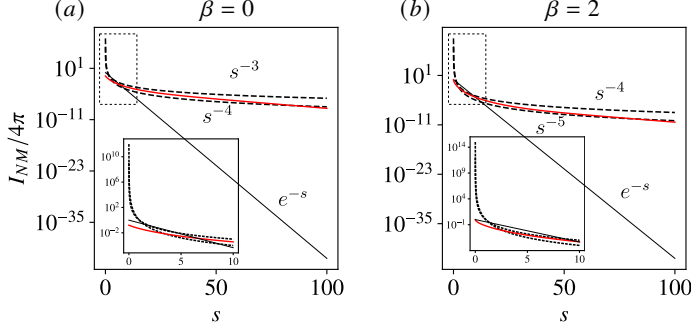


Figure 1: Comparison of the time correlation integral in (2.12) with e^{-s} , $1/s^3$, and $1/s^4$.

Exponentially decaying time correlation corresponds to Markovian vector potential.

Clearly, (2.1) defines a non-Markovian vector potential.

correlated white noise vector with zero mean and its correlation tensor is defined as

$$\langle \chi_i(\mathbf{x}, t) \chi_j(\mathbf{x} + \mathbf{r}, t + s) \rangle = 2\epsilon \delta_{ij} \delta(\mathbf{r}) \delta(s), \quad (2.2)$$

where ϵ is the intensity of the white noise and $(\hat{\cdot})$ denotes the respective quantities in the Fourier space. The solution of the vector potential in the Fourier space is given as

$$\hat{\eta}(\mathbf{k}, t) = \hat{\eta}(\mathbf{k}, 0) e^{-\frac{t}{\tau(\mathbf{k})}} + \int_0^t \frac{\hat{Q}(\mathbf{k})}{\tau(\mathbf{k})} \hat{\chi}(\mathbf{k}, t') e^{\frac{t-t'}{\tau(\mathbf{k})}} dt', \quad (2.3)$$

with the time correlation tensor defined as,

$$\langle \hat{\eta}_p^*(\mathbf{k}, t) \hat{\eta}_q(\mathbf{k}, t + s) \rangle = |\hat{Q}|^2 \frac{2\epsilon \delta_{pq} e^{-s/\tau(\mathbf{k})}}{(2\pi)^3 \tau(\mathbf{k})^2} \int_0^t \int_0^{t+s} \delta(t' - t'') e^{\frac{t'+t''-2t}{\tau(\mathbf{k})}} dt' dt''. \quad (2.4)$$

When, $t \rightarrow \infty$, the above expression yields,

$$\lim_{t \rightarrow \infty} \langle \hat{\eta}_p^*(\mathbf{k}, t) \hat{\eta}_q(\mathbf{k}, t + s) \rangle = \frac{2\epsilon \delta_{pq} |\hat{Q}|^2}{(2\pi)^3 \tau(\mathbf{k})} e^{-s/\tau(\mathbf{k})}. \quad (2.5)$$

To estimate the velocity auto-correlation time scale (decorrelation time for a particular scale) for synthetic fields, we substitute the above expression in

$$\phi_{ii}(\mathbf{k}, s) = \langle \hat{\mathbf{u}}^*(\mathbf{k}, t) \cdot \hat{\mathbf{u}}^*(\mathbf{k}, t + s) \rangle = k^2 \langle \hat{\eta}_p^* \hat{\eta}_q \rangle - k_m k_l \langle \hat{\eta}_m^* \hat{\eta}_l \rangle, \quad (2.6)$$

to obtain

$$\tau_c = \frac{\int_0^\infty \phi_{ii}(\mathbf{k}, s) ds}{\phi_{ii}(\mathbf{k}, 0)} = \tau(\mathbf{k}). \quad (2.7)$$

Equation (2.7) confirms that the decorrelation time scale of the velocity field at length scale $1/|\mathbf{k}|$ is quantified by $\tau(\mathbf{k})$. The auto-correlation of the Fourier transform of velocity $\phi_{ii}(\mathbf{k}, s)$ is related to the energy spectra $E(k)$ as (Batchelor 1953),

$$E(k) = 2\pi k^2 \phi_{ii} = \frac{k^4 \epsilon |\hat{Q}|^2}{\pi^2 \tau}, \quad (2.8)$$

where $k = |\mathbf{k}|$. A desired spatial variation in the kinetic energy spectrum is obtained using the filtering kernel $\hat{Q}(\mathbf{k})$ defined as

$$\hat{Q}_I(\mathbf{k}) = (1 + \ell^2 k^2)^{-n}, \quad (2.9)$$

where ℓ denotes a length scale. The subscript $(\cdot)_I$ denotes that this form of \hat{Q} is used for

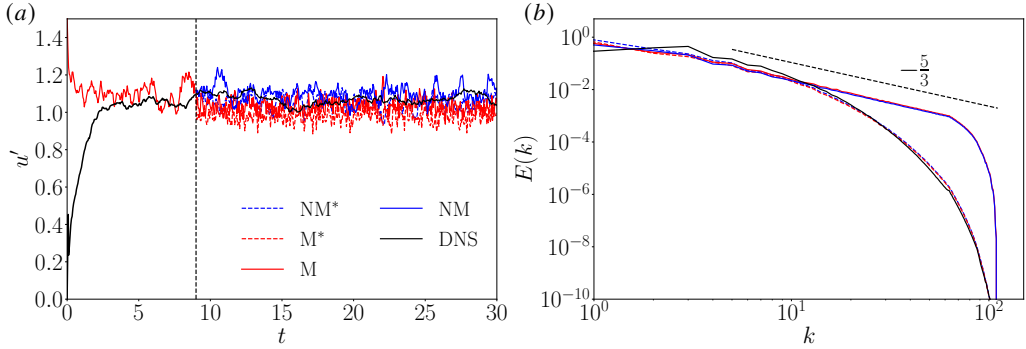


Figure 2: Comparison of (a) root mean square evolution for different velocity fields. (b) kinetic energy spectra for different velocity fields. For DNS, $k_{\max}\eta \approx 1.76$. The legends are the same for both figures.

	DNS	Markovian	Non-Markovian
Steady	DS1, DS2	MS1*, MS2, MS4, MS8, MS16*	NMS1*, NMS2, NMS4, NMS8, NMS16*
Decaying	DU1, DU2	MU1*, MU2, MU4, MU8, MU16*	NU1*, NMU2, NMU4, NMU8, NMU16*

Table 1: Parameter space for the simulations for both DNS and synthetic turbulent fields. The (*) indicates that the simulations were run for both ideal and matched spectra. The numbers in case names are equal to $1/\text{Sc}$ of the scalar.

achieving the so-called ideal spectra in our synthetic fields, i.e. $E(k) \sim k^{-5/3}$ for $\ell k \gg 1$. For varying $\tau(\mathbf{k})$ (not constant), the process $\boldsymbol{\eta}(\mathbf{x}, t)$ is a non-Markovian process. In the spatial domain, the time correlation is given by,

$$\langle \eta_p(\mathbf{x}, t) \eta_q(\mathbf{x} + \mathbf{r}, t + s) \rangle = \frac{1}{(2\pi)^3} \int_{\mathbb{R}^3} \langle \hat{\eta}_p^*(\mathbf{k}, t) \hat{\eta}_q(\mathbf{k}, t + s) \rangle e^{i\mathbf{k} \cdot \mathbf{r}} d\mathbf{k}, \quad (2.10)$$

which yields for $\hat{Q}_I(\mathbf{k})$ from (2.9),

$$C_{pq}^{\eta}(\mathbf{r}, s) = \langle \eta_p(\mathbf{x}, t) \eta_q(\mathbf{x} + \mathbf{r}, t + s) \rangle = \frac{2\epsilon\delta_{pq}}{(2\pi)^3} \int_{\mathbb{R}^3} \frac{(1 + \lambda^2 k^2)^{-2n}}{\tau(\mathbf{k})} e^{-s/\tau(\mathbf{k})} e^{i\mathbf{k} \cdot \mathbf{r}} d\mathbf{k}, \quad (2.11)$$

which resembles the correlation field studied by Chaves *et al.* (2003).

Equation (2.11) highlights that for varying $\tau(\mathbf{k})$, at a spatial point, $\boldsymbol{\eta}$ is a non-Markovian field since the integral can not be simplified to an exponentially decaying time correlation, unless $\tau(\mathbf{k}) = \text{constant}$ (the Markovian case). As we show in § 3, the velocity field generated due to Markovian $\boldsymbol{\eta}$ leads to weak scalar mixing, while the non-Markovian velocity field exhibits mixing dynamics very similar to turbulence. As shown in (2.7), $\tau(\mathbf{k})$ is the time after which velocity at scale $1/|\mathbf{k}|$ gets de-correlated with its history. In the context of hydrodynamic turbulence, $\tau(\mathbf{k})$ can be compared to the residence time of velocity perturbations at a particular length scale, before they get completely renewed. While the time scale for eddies at wavenumber k can be shown to be $\sim k^{-\frac{2}{3}}$ (Pope 2001), the so-called random sweeping effect (Gorbunova *et al.* 2021; Yeung & Sawford 2002; Wilczek & Narita 2012) results in $\tau \sim (u_0 k)^{-1}$ where u_0 is the large eddy velocity scale. Using a radial function for $\tau(\mathbf{k}) = 1/k$, and $n = 5/3$ in (2.9), we can simplify the integral in time correlations of

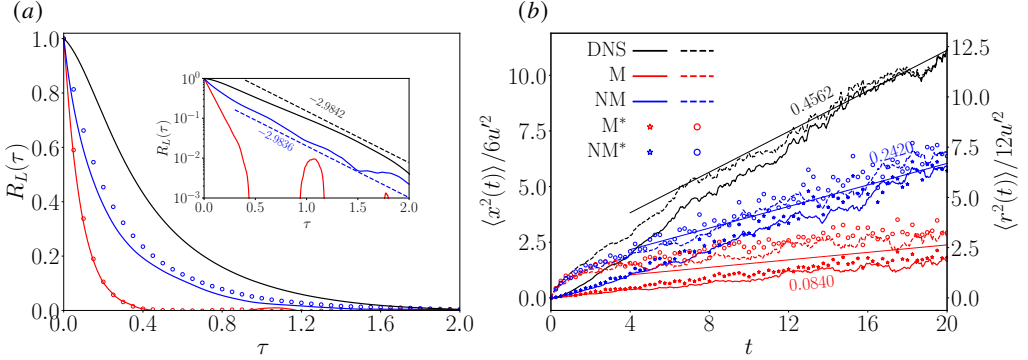


Figure 3: (a) The Lagrangian velocity correlations and (b) single particle (solid lines, empty stars) and pair (dashed lines, empty circles) dispersions for the Markovian, the non-Markovian, and the incompressible forced HIT simulations. T_L for DNS: 0.46, NM: 0.25, M: 0.08.

η , \mathbf{u} , and $\nabla \mathbf{u}$ as,

$$I_{NM}(s) = \frac{4\pi}{C} \int_0^\infty k^{\beta+3} \left(1 + \lambda^2 k^2\right)^{-\frac{10}{3}} e^{-ks} dk, \quad (2.12)$$

where $\beta = 0, 2, 4$ for η , \mathbf{u} , and $\nabla \mathbf{u}$, respectively. Figure 1 shows the variation of $I_{NM}/4\pi$ with s . The time correlation clearly decays slower than e^{-s} , thus confirming the non-Markovian nature of the η field, and consequently, that of \mathbf{u} and $\nabla \mathbf{u}$.

2.2. Numerical implementation and mixing simulations

Using the non-Markovian field developed above, and 3D incompressible DNS, we perform decaying and statistically stationary simulations of a passive scalar mixing. For numerical implementation of the synthetic fields, we follow Careta *et al.* (1994) and work with the time-discretized version of (2.3) to obtain

$$\hat{\eta}(\mathbf{k}, t + \Delta t) = \hat{\eta}(\mathbf{k}, t) e^{-\frac{\Delta t}{\tau(\mathbf{k})}} + \hat{Q}(\mathbf{k}) \alpha(\mathbf{k}, t) \sqrt{\frac{\epsilon}{2\tau(\mathbf{k})(2\pi)^3} \left(1 - e^{-\frac{2\Delta t}{\tau(\mathbf{k})}}\right)}, \quad (2.13)$$

where $\alpha(\mathbf{k})$ is also a delta-correlated Gaussian vector with unit intensity and $\hat{\eta}(\mathbf{k}, 0) = \sqrt{\epsilon/\tau} \hat{Q} \hat{\chi}$. We perform two sets of synthetic velocity mixing simulations: Markovian synthetic velocity field ($\tau(\mathbf{k}) = 0.1$ (const.)) and non-Markovian synthetic velocity field ($\tau(\mathbf{k}) = 1/k$). The value $\tau = 0.1$ for Markovian field is chosen to keep $E(k = 1)$ similar to DNS values (c.f. figure 2). Jossy *et al.* (2025) have shown that with $\tau = 0.01$ (\hat{Q} can be adjusted to keep suitable values of $E(k)$ as per (2.8)) fields mix very less. In the limit $\tau \rightarrow \infty$, we will obtain a steady field. It is noteworthy that the random sweeping approximation eliminates the arbitrariness related to the value of τ . For each of these sets, we run two further sets of simulations: statistically stationary scalar mixing with an imposed mean scalar gradient and decaying scalar mixing with an initialized spherical blob. To isolate the effect on mixing (if any), we further perform two sets of simulations for each: synthetic fields with ideal kinetic energy spectra of $k^{-5/3}$ using \hat{Q}_I defined in (2.9) and synthetic fields with kinetic energy spectra matched with our DNS simulations for which we use

$$\hat{Q}_M = \hat{Q}_I e^{-6.2 \left(\frac{k-10}{64\sqrt{3}-10}\right)^{1.05}}. \quad (2.14)$$

For comparing the mechanics of mixing by synthetic velocity fields, we perform 3D

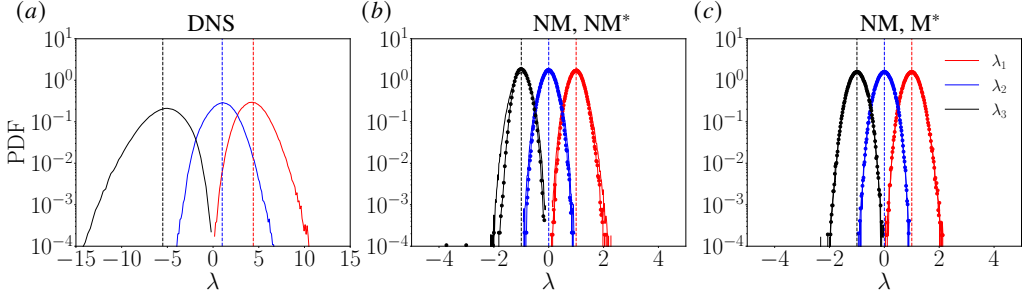


Figure 4: The distribution of the Lyapunov exponents for the DNS and the synthetic fields.

incompressible DNS of passive scalar mixing for both the decaying and statistically stationary mixing cases. We solve the forced incompressible Navier-Stokes equations,

$$\nabla \cdot \mathbf{u} = 0, \frac{D\mathbf{u}}{Dt} = -\nabla p + \frac{1}{\text{Re}} \nabla^2 \mathbf{u} + \mathbf{f}. \quad (2.15a)$$

All the simulations presented are performed with a 3D parallelized Fourier pseudo-spectral solver using P3DFFT++ library (Pekurovsky 2012) on a 192^3 grid with 2/3 dealiasing ($k_{\max} = 64$) in a $(2\pi)^3$ domain. In § 3, we also discuss Lagrangian tracking statistics, for which we use Lagrangian particle tracking implemented using PETSc (May & Knepley 2017). The forcing \mathbf{f} exists only in small wavenumbers $1 < k < 2\sqrt{3}$, governed by a process similar to (2.1) (Eswaran & Pope 1988). Synthetic velocity field simulations are done such that the turbulent kinetic energy κ and $u' = \sqrt{2\langle \kappa \rangle_x / 3}$ are similar as shown in figure 2(a), where $\langle \rangle_x$ denotes spatial average. figure 2(b) shows that the synthetic field is able to reproduce both the ideal and DNS energy spectra accurately. Velocity fields obtained either from DNS or from synthetic fields are used for mixing scalars governed by the equation,

$$\frac{D\phi}{Dt} = \frac{1}{\text{ReSc}} \nabla^2 \phi, \quad (2.16)$$

where Re is a characteristic Reynolds number and Sc is the Schmidt number. We perform DNS for only $\text{Sc} = 1$ and $1/2$ to save computational cost. In both synthetic and DNS runs, we use $\text{Re} = 125$.

3. Results

3.1. Lagrangian statistics

We calculate single particle correlation, pair dispersion, and the finite time Lyapunov exponents of Lagrangian particles in both the synthetic fields and compare them with those from DNS. Positions of the particles which follow the fluid streamlines are governed by,

$$\mathbf{x}^+(t) = \mathbf{X} + \int_0^t \mathbf{u}(\mathbf{x}^+(s); s) ds, \quad (3.1)$$

where \mathbf{X} denotes the initial location at $t = 0$. The single particle and velocity correlations are given by (Sawford 2012),

$$\langle \mathbf{u}^+(t) \cdot \mathbf{u}^+(t + \tau) \rangle = 2u'^2 R_L(\tau), \quad (3.2)$$

$$\langle \mathbf{x}^+(t) \cdot \mathbf{x}^+(t) \rangle - \langle \mathbf{x}^+(0) \cdot \mathbf{x}^+(0) \rangle = 6u'^2 \int_0^t \int_0^{t'} R_L(\tau) d\tau dt' = \langle x^2(t) \rangle, \quad (3.3)$$

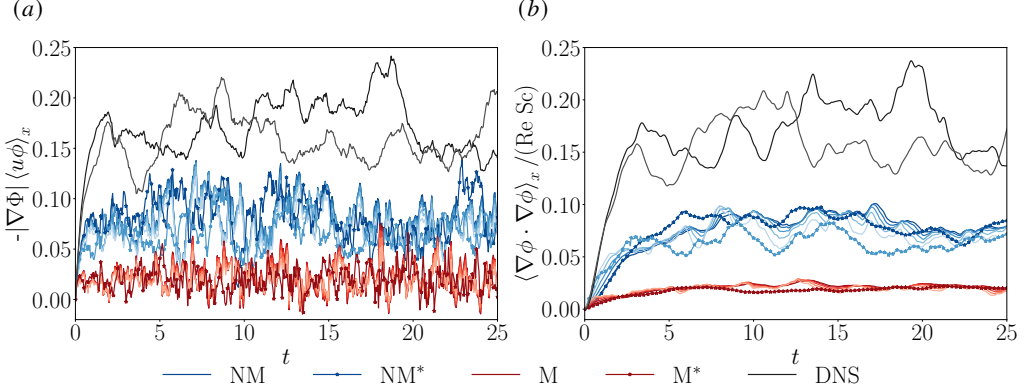


Figure 5: Timeseries of spatial average of (a) scalar production and (b) scalar dissipation for steady scalar mixing using DNS, non-Markovian, and Markovian velocity field for all Schmidt number cases.

using which, the Lagrangian integral time scale is defined as,

$$T_L = \int_0^\infty R_L(\tau) d\tau. \quad (3.4)$$

For $t \gg T_L$, the single particle correlation tends to $6u'^2 T_L t$. Similarly, pair dispersion can be computed using the separation between two particles,

$$\mathbf{r}^+ = \mathbf{x}^+ - \mathbf{y}^+ = \mathbf{X} - \mathbf{Y} + \int_0^t (\mathbf{u}(\mathbf{x}^+(s); s) - \mathbf{u}(\mathbf{y}^+(s); s)) ds. \quad (3.5)$$

For $t \gg T_L$, the position of the two particles become independent, hence $\langle |\mathbf{r}^+(t) - \mathbf{r}^+(0)|^2 \rangle \rightarrow 12u'^2 T_L = \langle r^2(t) \rangle$. Figure 3 summarizes these results. The non-Markovian velocity fields clearly exhibit Lagrangian integral time scales closer to the DNS compared to the Markovian fields for both ideal and matched spectra.

Based on the Lagrangian positions, we can define the deformation gradient at each particle (Ottino 1989) as,

$$\mathbf{F}(\mathbf{X}, t) = \nabla_{\mathbf{X}} \mathbf{x}^+, \quad (3.6)$$

which is related to the velocity gradient as,

$$\frac{d\mathbf{F}}{dt} = \nabla \mathbf{u}^+ \cdot \mathbf{F}, \quad (3.7)$$

where the Lagrangian velocity gradient is evaluated as $\nabla \mathbf{u}^+(t) = \nabla \mathbf{u}(\mathbf{x}^+(t); t)$. We track $\mathbf{F}(t)$ and its QR decomposition using a predictor-corrector time stepping (Götzfried *et al.* 2019) and compute the Finite Time Lyapunov Exponents (FTLE) of the fields. Figure 4 shows the distribution of the three Lyapunov exponents for the DNS and the synthetic fields. For DNS, the Lyapunov exponents approach the ratios $\langle \lambda_1 \rangle : \langle \lambda_2 \rangle : \langle \lambda_3 \rangle \approx 4.3 : 1 : -5.3$ using 64^3 particles for averaging. As discussed by Götzfried *et al.* (2019), an HIT field tends to compress a scalar inhomogeneity in one direction, pulling it in other direction. The largest and smallest exponents correspond to these deformations. The middle exponent, which is proportional to the triple velocity correlations (Balkovsky & Fouxon 1999) is non-zero due to the intermittency in the DNS. The overall kinematics result in a sheet-like structure forming from an otherwise concentrated inhomogeneity. Even though, the dispersion characteristics of the non-Markovian synthetic fields are closer to the DNS than the Markovian fields, due to

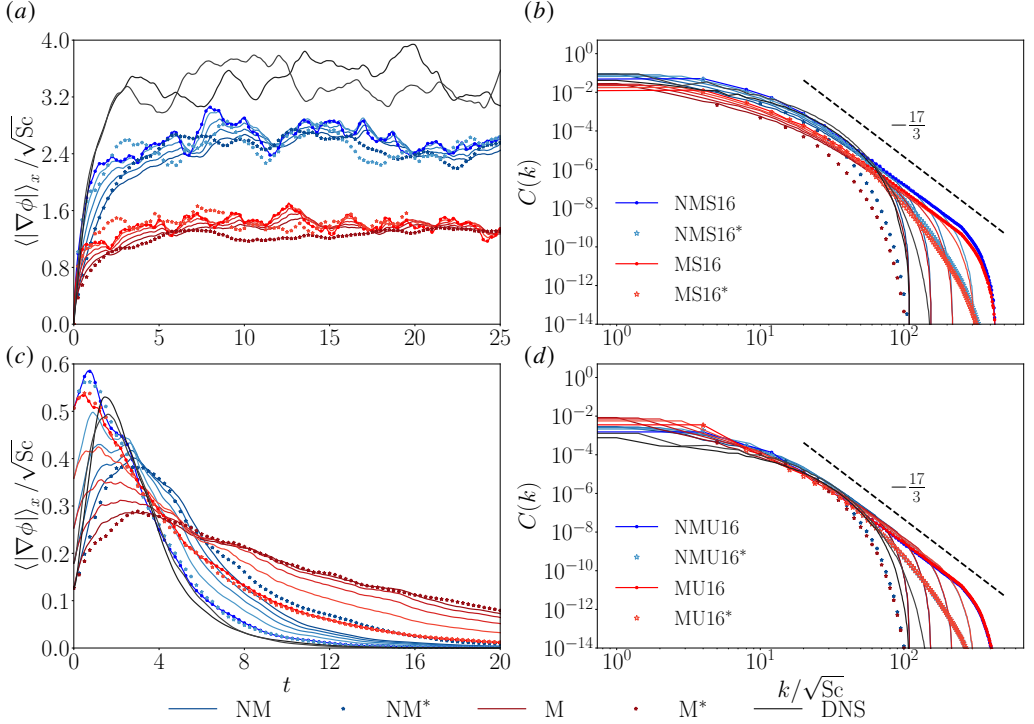


Figure 6: Time series of $\langle |\nabla \phi| \rangle_x$ for (a) stationary and (c) decaying case; (b) time-averaged scalar spectrum for steady scalar mixing and (d) scalar spectrum at $t = 3$ for decaying mixing with an arbitrary line of slope $-17/3$ for DNS, non-Markovian, Markovian velocity field for all Schmidt number cases.

their inherent Gaussian nature, the Lyapunov exponents for both the synthetic fields approach the ratios $\langle \lambda_1 \rangle : \langle \lambda_2 \rangle : \langle \lambda_3 \rangle \approx 1 : 0 : -1$, irrespective of the spectra.

3.2. Statistically stationary scalar field

We use the DNS and the synthetic fields to study mixing characteristics in a statistically stationary setup by solving for the concentration fluctuations assuming a constant mean gradient as,

$$\frac{D\phi}{Dt} = -\mathbf{u} \cdot \nabla \Phi + \frac{1}{ReSc} \nabla^2 \phi. \quad (3.8)$$

The corresponding scalar fluctuation variance equation is (Yeung & Sreenivasan 2014)

$$\frac{d}{dt} \frac{\langle \phi^2 \rangle_x}{2} = -\langle \mathbf{u} \phi \rangle_x \cdot \nabla \Phi - \frac{\langle |\nabla \phi|^2 \rangle_x}{ReSc}, \quad (3.9)$$

where $-\langle \mathbf{u} \phi \rangle_x \cdot \nabla \Phi$ is the production and $\langle |\nabla \phi|^2 \rangle_x / ReSc$ is the dissipation. In this work, we use $\nabla \Phi = (0.5, 0, 0)$. For spanning over different Schmidt numbers, we use the same synthetic field to save resources. The two DNS (DS1, DS2) are run independently. Figure 5 shows the time series of the production and the dissipation from all the simulations. The production (and hence the dissipation at the statistically stationary state) from the non-Markovian field is closer to the DNS than the Markovian field. Figure 6 shows the spatially averaged $|\nabla \phi|$ and the spectra of the scalar field, defined as $C(k) = |\hat{\phi}|^2 / 2$. As Sc decreases, the diffusive effects dominate the scalar mixing process. Consequently, the scalar field length

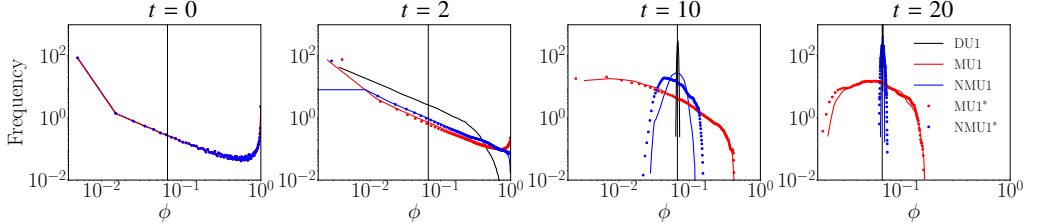


Figure 7: PDF of concentration at different time instances for DNS, non-Markovian and Markovian velocity field for $\text{Sc} = 1$ cases.

scale increases as $\sqrt{\text{Sc}}$ (given Re remains constant), as highlighted in figures 6b and d. At the statistically stationary state, the scalar spectra for both NM16 and M16 cases approach the $-17/3$ scaling law derived by Batchelor *et al.* (1959). This highlights the fact that the scalar spectrum exponent of $-17/3$ can be achieved even in a Markovian synthetic field as long as kinetic energy spectrum scales as $k^{-5/3}$.

3.3. Decaying mixing

To study mixing characteristics of a decaying case, we initialize the passive scalar concentration in a spherical blob defined as,

$$2\phi(\mathbf{x}, 0) = \tanh(5(S - \pi/2)), \quad (3.10)$$

where $S = \sqrt{(x - \pi)^2 + (y - \pi)^2 + (z - \pi)^2}$ and evolve using (2.16). Figures 6c, d show the spatially averaged $|\nabla\phi|$ and scalar spectra $C(k)$ for all the decaying cases. The time evolution of $\langle|\nabla\phi|\rangle_x$ in the non-Markovian cases matches the evolution observed in the DNS. On the other hand, in all the Markovian cases, the scalar gradients are sustained over a very long period of time denoting very low stirring of scalar field by the velocity field. This is also evident from the spatial histogram of the scalar concentration shown in figure 7, which highlight delayed homogenization due to Markovian fields, even though the scalar spectrum exponent approaches $-17/3$ for both the Markovian and the non-Markovian fields at large time. These results again show how non-Markovianity and the resulting spatiotemporal correlations of the synthetic velocity fields play a major role in the mixing process.

4. Conclusions

We have shown that non-Markovianity is an essential feature of turbulent flows, which can enhance turbulent mixing. Using an Ornstein-Uhlenbeck process with a different decorrelation time for each wavenumber, we demonstrated how a non-Markovian Gaussian velocity field can be used to improve the mixing properties of Markovian velocity models. Using the random-sweeping approximation, we use a decorrelation time inversely proportional to the wavenumber magnitude. We have shown that the time correlations of the synthetic velocity field thus obtained decay as τ^{-5} in a significant range of the time delay, thus confirming the non-Markovian nature of the velocity field. The Lagrangian velocity correlations, single particle correlations, and pair dispersions using the non-Markovian field are significantly closer to the DNS compared to the Markovian field. In the Eulerian description, scalars with all the Schmidt numbers exhibit better mixing properties (production in statistically stationary cases and mixing times in decaying blob mixing) with non-Markovian fields than the Markovian fields, though the exponent in scalar spectrum scales as $-17/3$ at low Schmidt numbers for both the fields.

Declaration of Interests. The authors report no conflict of interest.

REFERENCES

AREF, HASSAN 2020 Stirring by chaotic advection. In *Hamiltonian Dynamical Systems*, pp. 725–745. CRC Press.

BALKOVSKY, E & FOUXON, A 1999 Universal long-time properties of lagrangian statistics in the batchelor regime and their application to the passive scalar problem. *Physical Review E* **60** (4), 4164.

BATCHELOR, GK, HOWELLS, ID & TOWNSEND, AA 1959 Small-scale variation of convected quantities like temperature in turbulent fluid part 2. the case of large conductivity. *Journal of Fluid Mechanics* **5** (1), 134–139.

BATCHELOR, GEORGE KEITH 1953 *The theory of homogeneous turbulence*. Cambridge university press.

CARETA, A, SAGUÉS, F & SANCHO, JM 1994 Diffusion of passive scalars under stochastic convection. *Physics of Fluids* **6** (1), 349–355.

CHAVES, MARTA, GAWEDZKI, KRZYSZTOF, HORVAI, PETER, KUPIAINEN, ANTTI & VERGASSOLA, MASSIMO 2003 Lagrangian dispersion in gaussian self-similar velocity ensembles. *Journal of statistical physics* **113** (5), 643–692.

ESWARAN, VINAYAK & POPE, STEPHEN B 1988 An examination of forcing in direct numerical simulations of turbulence. *Computers & Fluids* **16** (3), 257–278.

GORBUNOVA, ANASTASIIA, BALARAC, GUILLAUME, CANET, LÉONIE, EYINK, GREGORY & ROSSETTO, VINCENT 2021 Spatio-temporal correlations in three-dimensional homogeneous and isotropic turbulence. *Physics of Fluids* **33** (4).

GÖTZFRIED, PAUL, EMRAN, MOHAMMAD S, VILLERMAUX, EMMANUEL & SCHUMACHER, JÖRG 2019 Comparison of lagrangian and eulerian frames of passive scalar turbulent mixing. *Physical Review Fluids* **4** (4), 044607.

HOLZER, MARK & SIGGIA, ERIC D 1994 Turbulent mixing of a passive scalar. *Physics of Fluids* **6** (5), 1820–1837.

JOSSY, JOAQUIM P, AWASTHI, PRATYUSH S & GUPTA, PRATEEK 2025 Active scalar mixing by homogeneous isotropic turbulence. *Physica D: Nonlinear Phenomena* p. 134926.

JOSSY, JOAQUIM P & GUPTA, PRATEEK 2025 Mixing of active scalars due to random weak shock waves in two dimensions. *Journal of Fluid Mechanics* **1007**, A25.

JUNEJA, A, LATHROP, DP, SREENIVASAN, KR & STOLOVITZKY, G 1994 Synthetic turbulence. *Physical Review E* **49** (6), 5179.

MAY, DAVE A & KNEPLEY, MATTHEW G 2017 Dmswarm: particles in petsc. In *EGU General Assembly Conference Abstracts*, p. 10133.

OTTINO, JULIO M 1989 *The kinematics of mixing: stretching, chaos, and transport*, , vol. 3. Cambridge university press.

PEKUROVSKY, DMITRY 2012 P3dfft: A framework for parallel computations of fourier transforms in three dimensions. *SIAM Journal on Scientific Computing* **34** (4), C192–C209.

POPE, STEPHEN B 2001 Turbulent flows. *Measurement Science and Technology* **12** (11), 2020–2021.

SAWFORD, BRIAN L 2012 4 a lagrangian view of turbulent dispersion and mixing brian l. sawford and jean-françois pinton. *Ten Chapters in Turbulence* p. 132.

TENNEKES, HENK 1975 Eulerian and lagrangian time microscales in isotropic turbulence. *Journal of Fluid Mechanics* **67** (3), 561–567.

TOUSSAINT, VALÉRIE, CARRIÈRE, PHILIPPE, SCOTT, JULIAN & GENCE, JEAN-NOËL 2000 Spectral decay of a passive scalar in chaotic mixing. *Physics of fluids* **12** (11), 2834–2844.

WILCZEK, MICHAEL & NARITA, YASUHITO 2012 Wave-number–frequency spectrum for turbulence from a random sweeping hypothesis with mean flow. *Physical Review E—Statistical, Nonlinear, and Soft Matter Physics* **86** (6), 066308.

YEUNG, PK & SAWFORD, BRIAN L 2002 Random-sweeping hypothesis for passive scalars in isotropic turbulence. *Journal of Fluid Mechanics* **459**, 129–138.

YEUNG, PK & SREENIVASAN, KR 2013 Spectrum of passive scalars of high molecular diffusivity in turbulent mixing. *Journal of Fluid Mechanics* **716**, R14.

YEUNG, PK & SREENIVASAN, KR 2014 Direct numerical simulation of turbulent mixing at very low schmidt number with a uniform mean gradient. *Physics of Fluids* **26** (1).

ZHOU, YE 2024 *Hydrodynamic Instabilities and Turbulence: Rayleigh–Taylor, Richtmyer–Meshkov, and Kelvin–Helmholtz Mixing*. Cambridge University Press.